The Pre submission synopsis (5000 words) is accepted and presentation was done accordingly. Recommended for final submission of the thesis

21/2/18 21/2/18 21/2/18 21/2/18 Arijit Roy 21/2/18

TECTONOTHERMAL HISTORY OF THE GRANULITES AND GNEISSES AROUND PHULBANI, ODISHA, INDIA AND ITS BEARING ON THE EVOLUTION OF THE PROTEROZOIC EASTERN GHATS BELT

Summary

By

PROLOY GANGULY

Registration no. - R-15RS15110001

PRESIDENCY UNIVERSITY
KOLKATA

Supervisor

Dr. Sankar Bose

2018

INTRODUCTION

Located at the eastern part of the peninsular India, Eastern Ghats Belt (EGB) is a Proterozoic orogenic belt which bears signature of attaining ultrahigh temperature metamorphism (UHT) at lower crustal condition. Among the very few worldwide occurrences of UHT terranes, EGB received international attention due to its complex geological history spanning over 1000 my which is linked to the evolution of the Proterozoic supercontinents Columbia and Rodinia (Dasgupta *et al*., 2017). The complex textural and micro-structural characters of high-grade rocks from this terrane provide crucial information on the processes that operate during anomalous thermal perturbation at lower crustal condition. Although it is clearly understood that the evolution of EGB is key to understand the Proterozoic orogenic system particularly involving India and East Antarctica, most of the geological records came from the central, western and southern part of EGB. The vastly exposed northern part of the terrane remains largely unexplored and very few petrological, structural and geochronological data are available. The present study is carried out on one such area, namely the Phulbani domain of the EGB where a detailed petrological, structural, fluid evolution and geochronological study has been carried out on a suite of granulite. The results of this study would not only help in understanding the geological evolution of the Phulbani domain of the EGB, but also correlate the major tectonothermal events from central part of EGB and its transcontinental neighbour in East Antarctica.

GEOLOGICAL BACKGROUND

EGB is conceived as a collage of several crustal provinces (namely, the Eastern Ghats Province, the Rengali Province, the Jeypore Province and the Krishna Province) and domains, each having its characteristic P-T-t histories and protolith characters (Ramakrishnan *et al.,* 1998; Rickers *et al.,* 2001; Dobmeier & Raith, 2003). Occurrences of UHT (>950°C) metamorphic rocks of deep crustal (8-10 kbar) origin have been reported from this belt (Lal *et al*., 1987; Sengupta *et al.,* 1990, 1999; Dasgupta *et al.,* 1995; Pal & Bose, 1997; Bose *et al.,* 2000; Das *et al.,* 2011; Korhonen *et al.,* 2013a; Sarkar & Schenk, 2014). High resolution geochronological data from this belt allowed a transcontinental correlation between India and East Antarctica, both of which are thought to be an integral part of the Proterozoic supercontinent Rodinia (Mezger & Cosca, 1999; Upadhyay *et al.,* 2009; Bose *et al.,* 2011, 2016; Das *et al.,* 2011; Korhonen *et al.,* 2013b). It has also been established that the central part of the EGB evolved through anticlockwise P-T path (Dasgupta & Sengupta, 2003; Korhonen *et al.,* 2013a; Dasgupta *et al.,* 2013). Geological history of the northern part of the

EGB is sketchy due to the poor account of geological data (cited in Dobmeier & Raith, 2003), excepting the Chilka Lake (Sen *et al.*, 1995; Bose *et al.*, 2016) and the Angul (Sarkar *et al.*, 2007) domains.

The central part of the Eastern Ghats Province (Domain 2 and part of Domain 3 of Rickers *et al.*, 2001) provides the maximum number of P-T-t data and it has a shared history with the Rayner Province of East Antarctica (reviewed in Dasgupta *et al.*, 2013, 2017; Harley *et al.*, 2013; Morissey *et al.*, 2015). However, crustal domains belonging to this province show contrasting styles of P-T-t evolution. While the well-studied Visakhapatnam domain is constituted of UHT metamorphosed rocks with a pronounced cooling history (Sengupta *et al.*, 1990; Dasgupta *et al.*, 1995; Bose *et al.*, 2000; Korhonen *et al.*, 2013a), the rocks of the Chilka Lake domain show a decompression-related P-T-t history (Sen *et al.*, 1995; Bose *et al.*, 2016). The time frame for UHT metamorphism and subsequent cooling in the former is ca. 1000-900 Ma (Upadhyay *et al.*, 2009; Bose *et al*., 2011; Das *et al.*, 2011; Korhonen *et al.*, 2013b), which is different from the ca. 780 Ma decompression in the latter (Bose *et al.*, 2016). The other domains of the Eastern Ghats Province, particularly occurring at the north of the Visakhapatnam domain include the Rampur domain, the Tikarpara domain, the Khariar domain, the Phulbani domain and the Angul domain. These domain names were coined by Dobmeier & Raith (2003) and their boundaries were drawn mostly from isotopic data of Rickers *et al.* (2001) along with discrete metamorphic ages across major lineaments that are interpreted as ductile shear zones (Dobmeier & Raith, 2003). Although few field data are available from such domain boundary shear zones (Chetty, 2010; Saha & Karmakar, 2015), others are identified mostly from satellite data (reviewed in Dobmeier & Raith, 2003). The significance of the ages showing distinct populations across the shear zones is also not clear. It is interpreted that these domains were amalgamated through the shear zones, yet the petrotectonic characters and the timings of the shearing events are mostly unknown. Needless to say, these domains have complex histories and a clear understanding of each one in the *P-T-D-t* space is required to gain a complete understanding of the evolution of the EGB.

The Phulbani domain which is focussed in the present study is interpreted to be separated from the westerly situated Rampur domain and the southerly placed Visakhapatnam domain by the combined Koraput-Sonapur and Nagavalli-Vamshadhara shear zones. Its northern boundary, shared with the Tikarpara domain, is marked by the Ranipathar shear zone while the eastern boundary, shared with the Chilka Lake domain, is marked by no prominent lineament. Barring some meagre geochronological data on aluminous granulite and charnockite (Paul *et al*. 1990; Upadhyay *et al*. 2009) no systematic analyses thus far have

been taken to understand the petrological evolution of this domain which creates difficulties to link the previously published geochronological data with the later. Therefore, detail petrological, geochronological and structural studies from Phulbani domain would be instrumental to understand the geological evolution of part of the northern EGB.

OBJECTIVE OF THE STUDY

The present work has been carried out with the following objectives:

1. To constrain the tectonothermal history of the high-grade rocks of Phulbani obtaining the petrological and structural evolution of the area.
2. To reveal the geochronological history of Phulbani and correlation of the same with the petrotectonic evolution of the area.
3. To propose a possible tectonic model for the evolutionary history of Phulbani.

LITHOLOGICAL AND STRUCTURAL CHARACTERS

The present study area is located in and around the Phulbani town, Kandhamal district, Odhisa, India (Fig. 1). The major lithological units are migmatitic felsic gneiss (garnet-quartz- K-feldspar-plagioclase-biotite gneiss), aluminous granulite (spinel-ilmenite-garnet-quartz-corundum-sillimanite ± K-feldspar ± plagioclase ± biotite gneiss), charnockite (K-feldspar-orthopyroxene-ilmenite-quartz-plagioclase-biotite ± garnet gneiss), felsic augen gneiss (garnet-quartz- K-feldspar-plagioclase-biotite gneiss) and calc-silicate granulite (scapolite-clinopyroxene-calcite-wollastonite-plagioclase-garnet-quartz gneiss). Locally mafic granulite (orthopyroxene-plagioclase-clinopyroxene-hornblende gneiss) is also present. Charnockite is subdivided into two types depending on the variation of the grain size and field relationships with other lithological units. Relatively fine-grained charnockite gneiss occurs as fragments and bands along with aluminous granulite (Fig. 2a), calc-silicate granulite and mafic granulite (Fig. 2b) within the felsic gneiss. On the other hand, the coarse-grained charnockite is intrusive in nature and contains fragments and lenses of calc-silicate granulite, aluminous granulite (Fig. 2c) and mafic granulite.

The rocks of the study area exhibit four generations of foliation. The earliest fabric (S_1) was developed during the D_1 deformation which is now preserved only at grain-scale (discussed later) as folded (F_2) inclusion trails of sillimanite, biotite and/or ilmenite within porphyroblastic corundum, spinel and garnet in the aluminous granulite. The resultant fabrics (S_2/S_3) of the subsequent deformations (D_2/D_3) are composite in nature because of the tight folding (F_3) of S_2 surface which gave rise to an axial planar S_3 fabric. This S_2/S_3 gneissic

fabric represents the macroscopically recognisable planar fabric in the aluminous granulite, the fine-grained charnockite gneiss and the migmatitic felsic gneiss occurring at the western part of the study area (Fig. 1). The S_2/S_3 gneissic fabric is characterized by alternate melanocratic and leucocratic layers in the aluminous granulite. Mineralogy of the melanocratic layers show wide variation in different locations and is dominantly defined by garnet-spinel-ilmenite-sillimanite-corundum ± biotite. Leucocratic layers are mainly constituted of quartz and feldspars, although sillimanite and biotite are occasionally present.

The S_2/S_3 fabric was subsequently transposed by the N-S to NW-SE trending S_4 fabric formed during the D_4 deformation which produced F_4 folds in macroscopic scale. The S_4 fabric is pervasive only at the central and the south-eastern parts of the study area and dominantly defined by the biotite ± sillimanite-bearing assemblages in the aluminous granulite, the felsic gneiss and the coarse-grained charnockite. In the south-eastern part of the study area, interference of F_3 (defined by S_2/S_3 gneissic foliation) and F_4 folds in the calc-silicate granulite produces non-plane cylindrical outcrop-scale fold interference pattern (Fig. 2d).

Discrete small-scale N-S trending steeply dipping ductile shear zones are present locally along the S_4 fabric at the central part and few other places of the study area. Localisation of mylonitic fabric (S_{4S}) along the ductile shear zones is conspicuous in the migmatitic felsic gneiss, the aluminous granulite and the associated coarse-grained charnockite (Fig. 2e). Sheared migmatitic layers of the aluminous granulite, present at the vertical sections within the ductile shear zone, confirm that the shear zone development occurred after the high-grade metamorphism. Shearing produced the S-C fabric in the aluminous granulite and the migmatitic felsic gneiss (Fig. 2f) with sinistral sense on plan view which is also confirmed by the asymmetry of garnet and feldspar porphyroclasts. Aluminous granulite and felsic gneiss locally preserve steeply southward plunging stretching lineation (Fig. 2g). Presence of shear fabrics in both the horizontal and the vertical sections suggests an oblique movement during development of these ductile shear zones.

At the northern part of the study area a broadly E-W trending brittle-ductile shear zone exists where mylonitic fabric and associated pseudotachylite veins are very conspicuous in aluminous granulite, migmatitic felsic gneiss, felsic augen gneiss and coarse-grained charnockite. According to the earlier workers (Dobmeier & Raith, 2003; Chetty, 2003) this shear zone is named as Ranipathar shear zone (RSZ). Structural mapping indicates that the earlier NW-SE trending S_4 fabric becomes folded at the vicinity of this shear zone (result of D_5 deformation) and within the shear zone it ultimately becomes parallel to the mylonitic

fabric (S_{5S}) which is indicative of transpressive movement along RSZ. Strong stretching lineations, present on such mylonitic foliation (S_{5S}), are defined by elongated quartz and feldspar grains in migmatitic felsic gneiss and felsic augen gneiss and by elongated quartz, feldspar and sillimanite grains in aluminous granulite. These stretching lineations are moderate to steeply north-easterly plunging. However down the dip stretching lineation is also notable at places. Within RSZ at some local low strain domains, traces of S_4 fabric is still preserved which is asymmetrically folded to give rise of dextral sense of movement on horizontal sections (Fig. 2h). In most cases the fold axes of such folds are steeply eastwardly plunging. Apart from this, S-C fabric and asymmetric tails of rotated porphyroclasts also indicate the dextral sense of shearing on plan view (Fig. 2i).

METHODOLOGY

Electron microprobe (EPMA) analysis

The chemical compositions of oxide, silicate and monazite in the aluminous granulite and the felsic gneiss were determined using a JEOL JXA 8200 Electron Probe Micro Analyzer (EPMA) at the Natural Science Center for Basic Research and Development (N-BARD), Hiroshima University, Japan. Chemical data for samples of the calc-silicate granulite, coarse-grained charnockite and fine-grained charnockite gneiss were analysed using CAMECA SX-100 EPMA at the Department of Geology and Geophysics, Indian Institute of Technology, Kharagpur, India. Operating conditions of both instruments were 15 kV accelerating voltage, 15 nA beam current and 2-3 μm beam diameter. Natural silicate and oxide standards were used for calibration in both instruments and the raw data were corrected using the ZAF program. During monazite analyses a standard monazite having ID-TIMS age of 1033 Ma (cited in Hokada & Motoyoshi, 2006) was used.

Sensitive High Resolution Ion Microprobe (SHRIMP) analysis

Zircon grains were selected and handpicked for mounting at Hiroshima University. Epoxy mounts were prepared with sample zircon grains and standard Duluth gabbroic anorthosite zircon (FC1) having an age of 1099±0.6 Ma (Paces & Miller, 1993). Subsequently, the mounts were polished and gold coated for observation under the JEOL Scanning Electron Microscope (SEM) at the Hiroshima University. Backscatter electron (BSE) and Cathodoluminescence (CL) imaging was done for each zircon grain to study the internal morphology as well as to decide the spot positions. Zircon analysis was done at the Hiroshima University with the SHRIMP IIe facility in two analytical sessions. External

zircon standard (SL13) was used to measure U contents. Raw data were processed using CONCH program (Nelson, 2006) while post-analysis data reduction was done based on the correction of the standard analyses. Each of the seven scans were checked and corrected and those with anomalous counts were rejected. The ages obtained by SHRIMP and EPMA are summarized in table 2.

Fluid inclusion analysis

Fluid inclusions were studied in doubly polished thin wafers (c. 200 µm in thickness) prepared from representative samples. The nature of occurrence of inclusions, their distribution patterns, shapes, sizes and phase categories were carefully studied and documented using a petrological microscope at varying magnifications using standard techniques (Touret, 2001; van den Kerkhof & Hein, 2001; van den Kerkhof *et al*., 2014). Microthermometric measurements were performed with a Linkam heating/freezing system at JAMSTEC, Yokosuka, Japan. Calibrations were undertaken with standard materials. Laser Raman spectroscopy was carried out using a Nano Photon Ltd Raman Touch spectrometer installed at JAMSTEC, Yokosuka, Japan. An exciting radiation at 532 nm was provided by a YAG laser. The analytical accuracy of wavenumber measurements of the Raman spectrometer was 1 wavenumber (cm^{-1}). Analyses were carried out on relatively large inclusions (>5 lm) to obtain good quality Raman signals. Raman data were acquired at room temperature for single-phase inclusions and compared with the data listed by Burke (2001) for fluids (CO_2, H_2O, CH_4, N_2, etc.) and solid crystals found in the inclusions to identify each species. The Raman bands for the host phases were compared with the Rruff database (http://rruff.info/) for precise identification.

Electron back-scattered diffraction (EBSD) analysis

Full crystallographic preferred orientation (CPO) of dynamically recrystallized quartz grains was measured from XZ thin sections using the electron back-scattered diffraction (EBSD) method. The EBSD patterns have been acquired using the Nordlys system attached to scanning electron microscope JEOL JSM6390A at Department of Earth and Planetary Systems Science, Hiroshima University, Japan with accelerating voltage of 15 KV and sample tilt of 70°. Obtained data were processed using HKL Channel 5.0 software package. The pole figures were plotted in equal area stereographic diagrams of the lower hemisphere with the trace of the mylonitic foliation (S) and stretching lineation (L) as reference directions.

PETROLOGICAL CHARACTERS

Aluminous granulite

The key textural features, mineral compositions and thermobarometric results obtained from aluminous granulite and the associated rocks are summarized in Table 1. The key minerals of the aluminous granulite are spinel (Spl), ilmenite (Ilm), magnetite (Mag), garnet (Grt), sillimanite (Sil), corundum (Crn), quartz (Qtz), K-feldspar (Kfs), plagioclase (Pl) and biotite (Bt). Mineral assemblage of this rock occur as strongly deformed layers (few cm- to mm-thick) that are engulfed within a quartzofeldspathic layer giving a migmatitic appearance of the rock. Within the aluminous granulite layers, spinel-corundum-garnet bearing micro-domains locally contain quartz, K-feldspar and biotite. However, there are domains where K-feldspar and matrix biotite are totally absent. Modal amount of plagioclase is low (~1%) in this rock. Depending on the presence of K-feldspar and matrix biotite, the aluminous granulite is subdivided into two mineral associations.

Association A is characterized by Spl, Ilm, Grt, Qtz, Kfs, Crn, Sil, Pl and Bt. Alternate layers of Grt-Spl-Crn-Ilm-Sil±Bt and Qtz-Kfs-Pl±Sil±Bt define the gneissic foliation (S_2/S_3). Porphyroblastic corundum (Crn_1) grains are usually rectangular in shape and coexist with porphyroblastic spinel (Spl_1: X_{Fe}-0.73 to 0.83) and ilmenite (Ilm_2). Inclusion trails (S_1) defined by early sillimanite (Sil_1) and biotite (Bt_1) are present within Crn_1, Spl_1 and Grt_1 (Fig. 3a). Coarse prismatic sillimanite grains (Sil_2) occur in the matrix. Skeletal intergrowth of spinel (Spl_2: X_{Fe}-0.70 to 0.72) and Qtz develops over Grt_1 (X_{Fe}: 0.74 to 0.84) and Sil_2 grains within the Grt-Spl-Crn-Ilm-Sil±Bt layers which are tightly folded to form the composite S_2/S_3 gneissic fabric. A double-layer corona of sillimanite (Sil_3) and garnet (Grt_2: X_{Fe}: 0.76 to 0.80) separates the Spl_1 and Spl_2 from the matrix Qtz (Fig. 3b). Apart from the porphyroblastic variety, fine granular and vermicular corundum (Crn_2) lamellae are also present within Spl_1/Spl_2 and Grt_2 respectively. Intergrown biotite (Bt_2: X_{Fe}- 0.33 to 0.37) and sillimanite (Sil_4) locally wrap Grt_1 forming the S_4 fabric which overprinted the earlier S_2/S_3 gneissic fabric. It is important to mention that at some locale the S_4 fabric transformed into a mylonitic S_{4S} fabric. The double-layer corona of Sil_3 and Grt_2 in such a case shows extreme stretching along the S_{4S} mylonitic foliation (inset of Fig. 3b). S-C fabric is observed in planar sections cut parallel to the stretching lineation and perpendicular to the S_{4S} mylonitic foliation. Oriented grains of Sil_4, Bt_2 and stretched corona of Grt_2+Sil_3 constitute the C fabric whereas recrystallized quartz grains constitute the S fabric. Melt relics like

cuspate quartz grains, k-feldspar envelope over plagioclase etc. are present in this association of aluminous granulite.

Association B is devoid of K-feldspar, plagioclase and matrix biotite with very low modal proportion of quartz. It constitutes metre to centimetre-scale lenses within association A. Corundum grains show two modes of occurrences: (1) porphyroblastic Crn_1 with inclusions of fibrous Sil_1 and Bt_1, and (2) exsolved Crn_3 with Mag and Ilm_2 in a tripartite spinel-ilmenite-magnetite grain. Porphyroblastic spinel (Spl_1: X_{Fe}- 0.66 to 0.71) present in this rock are commonly associated with Ilm_2 as a part of the peak Fe-Ti-Mg-Al spinel solid solution. However, porphyroblastic variety of Spl_2 (X_{Fe} varies around 0.72) intergrown with Sil_2 replacing Crn_1 is also common.

In both the associations, porphyroblastic Crn_1 is separated from the matrix Qtz by thin corona of Sil_3 (Fig. 3c). However, double-layer corona of Sil_3 and Grt_2 are also present at the contacts between Crn_1 and matrix Qtz.

Migmatitic Felsic gneiss

The enclosing felsic gneiss is composed of quartz, K-feldspar, plagioclase and porphyroblastic garnet with minor amounts of plagioclase and shows microstructures of shearing. Sections of the felsic gneiss samples, cut parallel to X-Z plane of finite strain, show sporadic occurrences of the S-C structure (Fig. 3d). The S fabric is defined by elongated quartz grains showing recrystallization by subgrain rotation while the C fabric is defined by elongated feldspar and aggregate of biotite (X_{Fe}: 0.42 to 0.55) and sillimanite grains formed after porphyroblastic garnet (X_{Fe} = 0.78 to 0.81).

Coarse-grained charnockite

The coarse-grained charnockite contains K-feldspar, plagioclase, orthopyroxene, quartz, ilmenite, biotite with/without garnet and hornblende. It contains a gneissic foliation (S_4 and S_{4S}) in most places, but the rock also occurs as massive variety. In the foliated variety, dynamically recrystallized quartz and K-feldspar grains constitute the leucocratic layers. The melanocratic layers are composed of garnet, orthopyroxene, hornblende and biotite. Garnet ($Alm_{65-69}Py_{6-8}Grs_{21-24}Sp_{<3}$) occurs as corona with quartz at the contacts of orthopyroxene (X_{Mg} = 0.27-0.32) and/or ilmenite against plagioclase ($Ab_{50-52}An_{46-49}$) (Fig. 3e). Biotite (X_{Mg} = 0.60-0.62) and hornblende (X_{Mg} = 0.43-0.50) occur surrounding orthopyroxene.

Fine-grained charnockite gneiss

The fine-grained charnockite gneiss is composed of K-feldspar, plagioclase, orthopyroxene, ilmenite, quartz, garnet, hornblende and biotite. The gneissic foliation (S_2/S_3) of this rock is defined by the alternate melanocratic and leucocratic layers. Stretched orthopyroxene and ilmenite grains constitute the dark-coloured layers while the leucocratic layers are composed of quartz, K-feldspar and plagioclase. K-feldspar and plagioclase grains show granoblastic polygonal texture. Corona of garnet (+ quartz) is present around orthopyroxene and ilmenite at their contacts with plagioclase (Fig. 3f). These garnet grains are compositionally Fe-rich ($Alm_{72-74}Py_{3-4}Grs_{18-19}$) compared to that of the coarse-grained charnockite. Retrograde biotite (X_{Mg} = 0.43-0.47) and hornblende (X_{Mg} = 0.34-0.37) grains are present around orthopyroxene. Orthopyroxene is Al-poor (<1 wt% Al_2O_3) and Fe-rich (X_{Mg} = 0.16-0.19).

Calc-silicate granulite

The calc-silicate granulite is composed of scapolite (Scp), clinopyroxene (Cpx), wollastonite (Wo), garnet (Grt), plagioclase (Pl), calcite (Cal), quartz (Qtz) and titanite (Ttn). This rock is characterized by a prominent gneissosity (S_2/S_3) and the gneissic foliation is defined by alternate greenish and greyish layers (Fig. 3g). The greenish layers are composed of Scp, Cpx, Pl, Cal with/without Qtz showing granoblastic texture whereas thin garnet corona develops surrounding Scp, Cpx, Pl, Cal and Wo in the greyish layer (Fig. 3h). Garnet composition is grossular-andradite-almandine solid solution with insignificant pyrope and spessartine components. Compositional variation exists in terms of andradite (13-29 mole%) and grossular (69-84 mole%) components. Scapolite is meionitic with X_{Mei} varying within the range of 0.80-0.83. Plagioclase is almost pure anorthite (96 to 99 mole% An). Clinopyroxene is dominantly diopside-hedenbergite solid solution with wide variation of X_{Mg} (0.50-0.63). A rim-ward decrease of Mg and corresponding increase of Fe^{2+} has been noted in porphyroblastic grains surrounded by garnet corona.

Felsic augen gneiss

This rock is exposed only at the vicinity of the Ranipathar shear zone. This rock contains porphyroclasts of perthitic feldspar that occur as augen within a recrystallized quartzofeldspathic matrix where biotite is occasionally present. Garnet is sporadic in appearance and occurs as porphyroblastic phase. Apatite, zircon and monazite occur as accessory minerals. This rock has the appearance of porphyritic granite when it occurs away

from the Ranipathar shear zone. While within the shear zone, it shows pervasive deformation with the development of a broadly E-W trending mylonitic foliation (S_{5S}).

GEOTHERMOBAROMETRY AND PHASE DIAGRAM MODELLING

The peak temperature of metamorphism (M_2) is estimated from Spl_1-Sil_3-Grt_2-Qtz assemblage (Nichols *et al.*, 1992) of aluminous granulite and varies within the range of 917-964ºC. From the same rock the peak pressure is estimated to be 8.0-8.2 kbar using the Grt_1-Spl_2-Sil_2-Qtz assemblage (Bohlen et al., 1986). For the felsic gneiss sample, the estimated peak pressure is 7.4-8.6 kbar using the garnet-aluminosilicate-silica-plagioclase barometer (Newton & Haselton, 1981). The temperature for the retrograde stage (late M_{2R} stage of metamorphism) was constrained by Fe-Mg exchange thermometer of Ganguly *et al.* (1996) considering ion exchange was occurred between matrix biotite (Bt_2 in aluminous granulite) and porphyroblastic garnet (Grt_1 in aluminous granulite) in association A of the aluminous granulite and the felsic gneiss. Using this thermometer the temperature is estimated to be 643-679°C and 468-680°C respectively for the association A of aluminous granulite and the felsic gneiss. In the latter case, the higher (e.g. 680°C) and lower (e.g. 468°C) temperatures were calculated using the core and rim compositions of garnet. Using the Ti-in-biotite thermometer (Henry *et al.*, 2005), the temperatures are estimated to be up to 790°C and 713°C respectively for the association A and the felsic gneiss.

In calc-silicate granulite the scapolite (meionite) composition with X_{Mei} of 0.80-83 suggests temperature in excess of 800°C (Harley, 1989). The garnet-orthopyroxene-plagioclase-quartz thermobarometry of Pattison *et al.* (2003) that takes into account the late Fe^{2+}-Mg exchange, yielded temperatures of 681-693°C and pressure of 6.2 kbar in coarse-grained charnockite. Using the same model, the temperatures were estimated to be within 735-770°C and the pressure within 6.4-6.8 kbar for the fine-grained charnockite gneiss. In both cases, higher temperatures were estimated using the core compositions of orthopyroxene grains. The estimated pressure is slightly lower (ΔP= 1.5 kbar) compared to the pressure estimated for the peak M_2 metamorphism constrained from spinel bearing assemblage of aluminous granulite.

Phase diagram modelling of the Si-undersaturated aluminous granulite was done in perple_x 6.7.5 (Connolly & Petrini, 2002; Connolly, 2005, 2009) using the internally consistent thermodynamic database of Holland and Powell (2011). As the experimental data on phase relationships for Mg-Fe-Al rich Si-undersaturated bulk rock is limited (e.g. Shulters

& Bohlen, 1989) the phase diagram modelling proved to be instrumental in the present study to constrain the pre-peak to post-peak evolution of the aluminous granulite.

Phase diagram calculation was done in the FeO-MgO-Al_2O_3-SiO_2-TiO_2-MnO-O_2 (FMASTMnO) system for association B and in the Na_2O-CaO-K_2O-FeO-MgO-Al_2O_3-SiO_2-H_2O-TiO_2-MnO-O_2 (NCKFMASHTMnO) system for association A to account the *P-T* evolution of the aluminous granulite. Phase diagram modelling for both the above associations suggest that although co-occurring within the same sample, corundum and quartz became stable at two different temperature windows. The corundum-bearing assemblage (pre-M_2) was stable up to 800ºC and the quartz-bearing assemblage (peak M_2) became stable only above 950ºC at 8kbar pressure (Fig. 4). Thus, collating the phase diagram and textural study of the aluminous granulite it is inferred that the shift from the corundum- to quartz-bearing assemblage was governed by two back-to-back reactions viz. garnet + corundum = spinel + sillimanite and garnet + sillimanite = spinel + quartz during prograde heating. It is worth noting that the later reaction marks the onset of UHT metamorphism within the aluminous granulite and produced spinel and quartz which reacted with each other to develop coronal garnet and sillimanite during cooling (M_{2R}) after attainment of UHT condition.

FLUID INCLUSION STUDY

Fluid inclusions which are present within the reported rocks were analyzed to understand the character of fluid during UHT metamorphism. Both Primary and secondary fluid inclusions occur within garnet, K-feldspar, quartz and plagioclase (Figs. 5a, 5b, 5c). Mono-phase primary fluid inclusions are circular to oblong augen shaped in most cases and locally concentrated or disseminated within the host mineral grains. T_m and T_h of these fluid inclusions vary within the range of -57.4 to -61.6 °C and -19 to 7.6 °C respectively. The secondary and pseudosecondary fluid inclusions are trail-bound and T_m of these fluid inclusions vary within the range of -58.2 to -58.5 °C and -57.8 to -58.7 °C respectively. T_h of the secondary and the pseudosecondary fluid inclusions are much higher than the primary inclusions and yield a temperature range of 7.6 to 19.7 °C and 15 to 27.2°C. Raman spectra of all the inclusions indicate that these are dominantly CO_2. However, minor amount of N_2, Ch_4 and H_2O are also present as suggested by minor peaks in Raman spectra. The maximum density of the primary fluid inclusions is calculated to be around 1.03 gm/cc which is much higher than the calculated density of the secondary (0.77 to 0.88 gm/cc) and the pseudosecondary (0.74 to 0.82 gm/cc) inclusions.

GEOCHRONOLOGY

Aluminous granulite

The $^{207}Pb/^{206}Pb$ date from the analysed zircon grains lie within the range 1026±10 to 900±9 Ma which dominantly belongs to the moderate- to dark- CL homogeneous core regions. However, a much older highly discordant $^{207}Pb/^{206}Pb$ date of 1765±5 Ma was also calculated from this region. A single analysis from the bright-CL xenocrystic core yields concordant $^{207}Pb/^{206}Pb$ date of 1136±14 Ma (Fig. 6a).

Spot dates from the included monazite grains and the Th-rich core of the matrix monazite grains constitute populations with weighted mean ages of 984±7 Ma and 997±13 Ma (Fig. 7a). Another group of data yields a weighted mean age of 966±4 Ma from the Th-rich cores of the matrix monazite grains. Three distinct populations having weighted mean ages of 939±10 Ma, 894±13 Ma and 781±15 were calculated from the overgrowth domains of the matrix monazite grains. The latter two age domains are located only at the Y-rich rims of the matrix monazite grains. A single spot from the exterior part of matrix monazite gives 701±39 Ma date.

Migmatitic felsic gneiss

The $^{207}Pb/^{206}Pb$ dates of the zircon grains lie within the range of 1133 ± 22 to 863±13 Ma. It is important to note that while the older dates (1133 ± 22 Ma and 1117 ± 24 Ma) belong to the xenocrystic cores, the younger dates dominantly come from the prismatic cores and overgrowth domains. The prismatic cores and the overgrowth domains yield $^{207}Pb/^{206}Pb$ spot dates within the range of 976±7 Ma to 983 ± 20 Ma and 863±13 Ma to 987±14 Ma (Fig. 6b).

From the analysed monazite grains, two distinct age populations were noted. An older age of 968±4 Ma is calculated from data points dominantly from the Th-rich oscillatory zoned cores (Fig. 7b). However, the Y-rich patches also contain spot dates belong to this ca. 968 Ma. Spot dates that define a younger age of 942±10 Ma are only present at the Y-rich patches. These two populations are analogous to the mean ages of 966±4 Ma and 939±10 Ma calculated from the aluminous granulite. No younger population was noted except a single spot date of 885±24 Ma.

Charnockite

Most of the zircon grains of coarse-grained charnockite are characterized by oscillatory zoning. Data from these oscillatory zoned domains yield mean $^{207}Pb/^{206}Pb$ ages of 967±5 Ma and 971±18 Ma (Fig. 6c, 6d). Additionally, relatively younger group ages of 967±20 Ma and

947±8 Ma are also calculated from the same domains. Additionally ca. 915-960 Ma spot dates from the overgrowth domains perhaps reflect the age of metamorphism subsequent to the emplacement of the protolith of this rock.

Analyzed zircon grains of the fine-grained charnockite gneiss yield age ranges between 1190±18 Ma to 947±9 Ma (Fig. 6e). Of this age spectrum, relatively older spot dates of 1190±18Ma and 1165±25 Ma were calculated from two xenocrystic cores. Apart from this the other spot dates that belong to the prismatic core domains vary within the range of 1024±6 Ma to 958±10 Ma. The overgrowth domains that occurs either around the xenocrystic or prismatic cores yield age ranges between 1156±6 to 947±9 Ma.

Felsic augen gneiss

Majority of the zircon grains of this sample is euhedral and characterized by very conspicuous oscillatory zoning. A mean $^{207}Pb/^{206}Pb$ age of 1169±8 Ma is obtained from the oscillatory zoned cores (Fig. 6f). A single spot analysis from the portion that covers area from both the oscillatory zoned core domain yields $^{207}Pb/^{206}Pb$ date of 1038±13 Ma. A much younger $^{207}Pb/^{206}Pb$ age of 977±11 Ma is also calculated from the dark-CL central part of a zircon grain.

ELECTRON BACKSCATTERED DIFFRACTION (EBSD) STUDY

The XZ section of migmatitic felsic gneiss having the S_{4S} mylonitic foliation was analysed by SEM-EBSD technique to constrain the CPO patterns of the deformed quartz grains and to derive the temperature of D_4 deformation. The c-axis pole figures of the quartz grains (Fig. 8) of the sheared migmatitic felsic gneiss samples consistently have maxima near the centre which indicate dominant deformation by dislocation creep on prism <a> slip. Moreover, in band contrast image the grain boundaries of the equidimensional quartz grains are very prominent and individual grains have large misorientation (greater than 10º) relative to the adjacent grains which suggest that subgrain rotation recrystallization of the quartz grains leading to the development of equidimensional new grains.

DISCUSSION

P-T-D-fluid evolution

Integration of field, textural and thermobarometric data suggests that the Si-undersaturated aluminous granulite suffered UHT metamorphism (M_2 at ~1000ºC, 8-8.5 kbar) followed by

near-isobaric cooling (M_{2R}) (down to 680°C) along a near-isobaric prograde and retrograde path (Fig. 9). Phase diagram modelling shows that the switchover from a corundum-bearing assemblage (pre-M_2) to a quartz-bearing assemblage at the peak metamorphic condition (M_2) was controlled by progressive heating. Pressure-temperature data estimated from the associated calc-silicate granulite also indicate attainment of >800°C temperature at the peak M_2 metamorphic stage. Regionally recognizable composite S_2/S_3 gneissic fabrics (result of D_2/D_3) developed during the attainment of this peak metamorphism. The appearance of sillimanite + garnet corona over spinel (aluminous granulite) and garnet corona over scapolite, clinopyroxene, plagioclase and wollastonite (calc-silicate granulite) suggests an event of near-isobaric cooling (M_{2R}) from the peak. The garnet (with intergrown quartz) corona over orthopyroxene and ilmenite against plagioclase in both varieties of charnockite also indicates cooling from a temperature >800°C. During this cooling period biotite- and sillimanite-bearing assemblage developed in aluminous granulite and migmatitic felsic gneiss to form the $S_{4/4S}$ and S_{5S} fabrics (result of D_4 and D_5). The Garnet-biotite Fe-Mg exchange thermometry from the samples containing these fabrics yield temperature ranges between 468 to 680°C possibly suggesting that the development of these occurred at amphibolite grade. Additionally the dominant presence of prism <a> slip within the quartz grains of migmatitic felsic gneiss suggest that the D_4 deformation occurred around 500°C (Passchier & Trouw, 2005) which simply corroborates the result obtained by the Fe-Mg exchange thermometer.

Fluid inclusion data from the representative samples reveal that all the rocks equilibrated with a CO_2-rich fluid during the peak metamorphism. The primary fluid inclusions in the coarse-grained charnockite are also CO_2-rich. Since the coarse-grained charnockite was emplaced subsequent to the M_2 stage (post-UHT), it implies that CO_2-rich fluid was present even after the UHT metamorphism. Lower density of the secondary and pseudosecondary fluid inclusions in some samples indicates that entrapment of these inclusions occurred during upliftment of the cooled lower crust.

Geochronological evolution

$^{207}Pb/^{206}Pb$ mean age of 1169±8 Ma from the oscillatory zoned zircon cores of the felsic augen gneiss within the Ranipathar shear zone possibly suggests the crystallization age of this granitic rock. Additionally, spot dates of 1038±13 Ma 977±11 Ma perhaps represents a metamorphic event during this time. It is possible that the granitic rock (now felsic augen gneiss) from the Ranipathar shear zone acted as a part of the basement of the Eastern Ghats Province. Presence of 1190±18 Ma spot dates in the xenocrystic zircon cores of the fine-

grained charnockite gneiss could also be correlated with the ca. 1169 Ma emplacement age of the protolith of the augen gneiss mentioned above.

Texturally constrained in-situ monazite ages of 997±13 Ma and 984±7 Ma from the aluminous granulite could represent the time span of UHT metamorphism (M_2) and regionally recognizable S_2/S_3 fabric forming event at Phulbani domain. Near-concordant spot dates of 1000±9 Ma from the aluminous granulite and 1012±8 Ma and 1024±6 Ma from fine-grained charnockite gneiss, perhaps bearing the traces of the UHT metamorphism. These spot dates match well with the age of UHT metamorphism from the adjacent Visakhapatnam domain (Bose *et al*., 2011; Das *et al*., 2011). Zircon spot dates spanning ca. 980-960 Ma from aluminous granulite, fine grained charnockite and the migmatitic felsic gneiss of the present study could be the age of final stage melt crystallization. Group ages of 966±4 Ma and 968±4 Ma retrieved from the peripheral part of the included monazite grains and from the matrix of the aluminous granulite and migmatitic felsic gneiss possibly signify the cooling age following the UHT metamorphism.

Presence of aluminous granulite and calc-silicate granulite fragments within the coarse-grained charnockite indicate that chranockite plutonism occurred after UHT metamorphism. Mean ages of 967±5 Ma and 971±18 Ma from oscillatory zoned zircon grains of two samples of the coarse-grained charnockite suggest crystallization ages for charnockite magma.

The spread of dates between ca. 960 to 900 Ma recorded from zircon and mean ages of 939±10 Ma and 894±13 Ma from monazite of aluminous granulite might be linked to important events within the Eastern Ghats Province. These two could be related to ca. 950 Ma and ca. 900 Ma ages reported from the Visakhapatnam domain (Bose et al., 2011; Das et al., 2011) which are considered as age of reworking of the cooled UHT rocks and final stage of melt crystallization respectively. In both the above domains zircon ages younger than ca. 900 Ma is absent which lead to the idea that both of these domains possibly entered into a tectonically quiescent period during that time. However, Phulbani domain perhaps witnessed episodic shearing activity that remobilized and eventually exhumed the cooled UHT metamorphosed crust. In this context, group age of 781±15 Ma from matrix monazite grains of aluminous granulite of the present study could be the age of ductile shearing (D_4/ S_{4S}).

CONCLUSIONS

1. Textural, thermobarometric and theoretical data suggest that Phulbani domain experienced a near isobaric prograde and retrograde P-T evolution with peak UHT metamorphism (ca.1000ºC at 8-8.5 kbar) that was followed by isobaric cooling.
2. A CO_2-rich fluid phase was present throughout the evolution of the lower crust, encompassing UHT metamorphism, charnockite emplacement and subsequent cooling.
3. Felsic augen gneiss of the present study formed at ca. 1169 Ma and possibly provided the basement for deposition of sediment which later on experienced UHT metamorphism (aluminous granulite and calc-silicate granulite of the present study) during ca. 997-984 Ma. Spot dates of ca. 1012 Ma, 1024 Ma from fine-grained charnockite gneiss and ca. 1026 Ma from aluminous granulite possibly bear the glimpses of early stage of UHT metamorphism. Protracted period of charnockite plutonism occurred at ca. 967 and ca. 971 Ma following the UHT metamorphism.
4. Similar metamorphic and geochronological evolutionary history of Phulbani and adjacent Visakhapatnam domains vindicate the possibility of these two to be contiguous during ca. 1000-900 Ma posing questions on the validity of domain-based classification of Eastern Ghats Province.

FUNDING

The author acknowledges financial supports from the University Grants Commission (UGC) Govt. of India through a research fellowship (Sanction No. F.11-15/2003 SA-I).

REFERENCES

Bohlen, S. L., Dollase, W. A. & Wall, V. J. (1986). Calibration and applications of spinel equilibria in the system FeO-Al_2O_3-SiO_2. *Journal of Petrology* **27**, 1143-1156.

Bose, S., Fukuoka, M., Sengupta, P. & Dasgupta, S. (2000). Evolution of high Mg-Al granulites from Sunkarametta, Eastern Ghats, India: evidence for a lower crustal heating-cooling trajectory. *Journal of Metamorphic Geology* **18**, 223-240.

Bose, S., Dunkley, D. J., Dasgupta, S., Das, K. & Arima, M. (2011). India-Antarctica-Australia-Laurentia connection in the Paleo-Mesoproterozoic revisited: evidence from new zircon U–Pb and monazite chemical age data from the Eastern Ghats Belt, India. *Geological Society America Bulletin* **123**, 2031-2049.

Bose, S., Das, K., Torimoto, J., Arima, M. & Dunkley, D. J. (2016). Evolution of the Chilka Lake granulite complex, northern Eastern Ghats Belt, India: First evidence of ~780Ma decompression of the deep crust and its implication on the India-Antarctica correlation. *Lithos* **263**, 161-189.

Burke, E. A. J. (2001). Raman microspectrometry of fluid inclusions. *Lithos* **55**, 139-158.

Chetty, T. R. K., Vijay, P., Narayana, B. L. & Giridhar, G. V. (2003). Structure of the Nagavali shear zone, Eastern Ghats Mobile Belt, India: correlation in the East Gondwana reconstruction. *Gondwana Research* **6**, 215-229.

Chetty, T. R. K. (2010). Structural architecture of the northern composite terrane, the Eastern Ghats Mobile Belt, India: Implications for Gondwana tectonics. *Gondwana Research* **18**, 565-582.

Connolly, J. A. D. (2005). Computation of phase equilibria by linear programming: a tool for geodynamic modelling and its application to subduction zone decarbonation. *Earth and Planetary Science Letters* **236**, 524–541.

Connolly, J. A. D. (2009). The geodynamic equation of state: what and how. *Geochemistry, Geophysics, Geosystems* **10**, Q10014.

Connolly, J. A. D. & Petrini, K. (2002). An automated strategy for calculation of phase diagram sections and retrieval of rock properties as a function of physical conditions. *Journal of Metamorphic Geology* **20**, 697-708.

Das, K., Bose, S., Karmakar, S., Dunkley, D. J. & Dasgupta, S. (2011). Multiple tectonometamorphic imprints in the lower crust: first evidence of *ca. 950 Ma* (zircon U-Pb SHRIMP) compressional reworking of UHT aluminous granulites from the Eastern Ghats Belt, India. *Geological Journal* **46**, 217-239.

Dasgupta, S. & Sengupta, P. (2003). Indo-Antarctic correlation: a perspective from the Eastern Ghats granulite belt, India. In: Yoshida, M., Windley, B.F. & Dasgupta, S. (eds.) Proterozoic East Gondwana: supercontinent assembly and breakup. *Geological Society London Special Publications* **206**, 131-143.

Dasgupta, S., Bose, S. & Das, K. (2013). Tectonic evolution of the Eastern Ghats Belt. *Precambrian Research* **227**, 247-258.

Dasgupta, S., Bose, S., Bhowmik, S.K. & Sengupta, P. (2017). The Eastern Ghats Belt, India, in the context of supercontinent assembly. In: Dasgupta, S. & Pant, N.C. (eds.*)* Crustal evolution of India and Antarctica: the supercontinent connection. *Geological Society London Special Publications* **457**, https://doi.org/10.1144/SP457.5.

Dasgupta, S., Sengupta, P., Ehl, J., Raith, M. & Bardhan, S. (1995). Reaction textures in a suite of spinel granulites from the Eastern Ghats Belt, India: evidence for polymetamorphism, a partial petrogenetic grid in the system KFMASH and the roles of ZnO and Fe_2O_3. *Journal of Petrology* **36**, 435-461.

Dobmeier, C. & Raith, M. M. (2003). Crustal architecture and evolution of the Eastern Ghats Belt and adjacent regions of India. In: Yoshida, M., Windley, B.F. & Dasgupta, S. (eds.) Proterozoic East Gondwana: supercontinent assembly and breakup. *Geological Society London Special Publication* **206**, 145–168.

Ganguly, J., Cheng, W. & Tirone, M. (1996). Thermodynamics of aluminosilicate garnet solid solution: new experimental data, an optimized model and thermometric applications. *Contributions to Mineralogy and Petrology* **126**, 137-151.

Harley, S. L. (1989). The origin of granulites: a metamorphic perspective. *Geological Magazine* **126**, 215-247.

Harley, S. L., Fitzsimons, I. C. W. & Zhao, Y. (2013). Antarctica and supercontinent evolution: historical perspectives, recent advances and unresolved issues. In: Harley, S. L., Fitzsimons, I. C. W. & Zhao, Y. (eds.) Antarctica and supercontinent evolution. *Geological Society London Special Publications* 383, 1-34.

Henry, D. J., Guidotti, C. V., Thomson, J. A. (2005). The Ti-saturation surface for low- to medium pressure metapelitic biotites: implications for geothermometry and Ti substitution mechanisms. *American Mineralogist* **90**, 316-328.

Hokada, T. & Motoyoshi, Y. (2006). Electron microprobe technique for U-Th-Pb and REE chemistry of monazite, and its implications for pre-, peak- and post-metamorphic events of the Lützow-Holm complex and the Napier complex, East Antarctica. *Polar Geoscience* **19**, 118–151.

Holland, T. J. B., & Powell, R. (2011). An improved and extended internally consistent thermodynamic dataset for phases of petrological interest, involving a new equation of state for solids. *Journal of Metamorphic Geology* **29**, 333-383.

Korhonen, F. J., Brown, M., Clark, C. & Bhattacharya, S. (2013a). Osumilite-melt interactions in ultrahigh temperature granulites: phase equilibria modelling and implications for the P-T-t evolution of the Eastern Ghats Province, India. *Journal of Metamorphic Geology* **31**, 881-907.

Korhonen, F. J., Clark, C., Brown, M., Bhattacharya, S. & Taylor, R. (2013b). How long-lived is ultrahigh temperature (UHT) metamorphism? Constraints from zircon and monazite geochronology in the Eastern Ghats orogenic belt, India. *Precambrian Research* **234**, 322-350.

Lal, R. K., Ackermand, D. & Upadhyay, H. (1987) P-T-X relationships deduced from corona textures in sapphirine–spinel–quartz assemblages from Paderu, southern India. *Journal of Petrology* **28**, 1139-1168.

Mezger, K. & Cosca, M. A. (1999). The thermal history of the Eastern Ghats Belt (India), as revealed by U–Pb and ^{40}Ar-^{39}Ar dating of metamorphic and magmatic minerals: implications for the SWEAT correlation. *Precambrian Research* **94**, 251-271.

Morissey, L. J., Hand, M. & Kelsey, D. E. (2015). Multi-stage metamorphism in the Rayner-Eastern Ghats Terrane: P-T-t constraints from the northern Prince Charles Mountains, east Antarctic. *Precambrian Research* **267**, 137-163.

Nelson, D. R. (2006). CONCH: a visual basic program for interactive processing of ion-microprobe analytical data. *Computers and Geosciences* **32**, 1479-1498.

Newton, R. C. & Haselton, H. T. (1981) Thermodynamics of the garnet-plagioclase-Al_2SiO_5-quartz geobarometers. In: Newton, R. C., Navrotsky, A. & Wood, B.J. (ed.) Thermodynamics of minerals and melts. *Advances in Physical Geochemistry* **1**, 131-147, Springer-Verlag.

Nichols, G. T., Berry, R. & Green, D. H. (1992). Internally consistent gahnitic spinel–cordierite-garnet equilibria in the FMASHZn system: geothermobarometry and applications. *Contributions to Mineralogy and Petrology* **111**, 362-377.

Paces, J.B. & Miller, J.D. (1993). Precise U-Pb ages of Duluth Complex and related mafic intrusions, northeastern Minnesota: geochronological insights to physical, petrogenetic, paleomagnetic and tectonomagmatic processes associated with the 1.1 Ga Mid-continent Rift System. *Journal of Geophysical Research* **98**, 13997-14013.

Pal, S. & Bose, S. (1997). Mineral reactions and geothermobarometry in a suite of granulite facies rocks from Paderu, Eastern Ghats granulite belt: A reappraisal of the P-T trajectory. *Proceedings of the Indian Academy of Sciences - Earth and Planetary Sciences* **106**, 77-89.

Paul, D.K., Ray Barman, T., McNaughton, N.J., Fletcher, I.R., Potts, P.J., Ramakrishnan, M. & Augustine, P. F. (1990). Archean-Proterozoic evolution of Indian charnockites: isotopic and geochemical evidence from granulites of the Eastern Ghats Belt. *The Journal of Geology* **98**, 253-263.

Passchier, C. W., & Trouw, R. A. (2005). *Microtectonics* (Vol. 1). Springer Science & Business Media.

Pattison, D. R. M., Chacko, T., Farquhar, J. & McFarlane, C. R. M. (2003). Temperatures of granulite facies metamorphism: constraints from experimental phase equilibria and thermobarometry corrected for retrograde exchange. *Journal of Petrology* **44**, 867-900.

Ramakrishnan, M., Nanda, J. K. & Augustin, P. (1998). Geological evolution of the Proterozoic Eastern Ghats mobile belt. In: Ramakrishnan, M., Paul, D.K., Mishra, R.N. (eds.) Geological evolution of Proterozoic Eastern Ghats Mobile Belt. *Geological Survey of India Special Publication* **44**, 1–21.

Rickers, K., Mezger, K. & Raith, M. M. (2001). Evolution of the continental crust in the Proterozoic Eastern Ghats Belt, and new constraints for Rodinia reconstruction: implications from Sm-Nd, Rb-Sr and Pb-Pb isotopes. *Precambrian Research* **112**, 183–212.

Saha, T. & Karmakar, S. (2015). Petrotectonic framework of granitoids and associated granulites at Nagavalli Shear Zone (NSZ), Eastern GhatsBelt: evidence of a late transpression orogeny. *Journal of Earth System Science* **124**, 707-727.

Sarkar, M., Gupta, S. & Panigrahi, M. (2007). Disentangling tectonic cycles along a multiply deformed terrane margin: Structural and metamorphic evidence for midcrustal reworking of the Angul granulite complex, Eastern Ghats Belt, India. *Journal of Structural Geology* **29**, 802-818.

Sarkar, T. & Schenk, V. (2014). Two-stage granulite formation in a Proterozoic island arc (Ongole domain of the Eastern Ghats Belt, India): Part 1. Petrology and pressure-temperature evolution. *Precambrian Research* **255**, 485-509.

Sen, S. K., Bhattacharya, S. & Acharyya, A. (1995). A multi-stage pressure–temperature record in the Chilka Lake granulites: the epitome of the metamorphic evolution of Eastern Ghats, India? *Journal of Metamorphic Geology* **14**, 287-298.

Sengupta, P., Dasgupta, S., Bhattacharya, P. K., Fukuoka, M., Chakraborti, S. & Bhowmik, S. (1990). Petro-tectonic imprints in the sapphirine granulites from Anantagiri, Eastern Ghats Mobile Belt, India. *Journal of Petrology* **31**, 971-996.

Sengupta, P., Sen, J., Dasgupta, S., Raith, M. M., Bhui, U. K. & Ehl, J. (1999). Ultra-high temperature metamorphism of metapelitic granulites from Kondapalle, Eastern Ghats Belt: implications for the Indo-Antarctic correlation. *Journal of Petrology* **40**, 1065-1087.

Shulters, J. C. & Bohlen, S. R. (1989). The Stability of hercynite and hercynite-gahnite spinels in corundum- or quartz-bearing assemblages. *Journal of Petrology* **30**, 1017-1031.

Touret, J. L. R. (2001). Fluid in metamorphic rocks. *Lithos* **55**, 1-25.

Upadhyay, D., Gerdes, A. & Raith, M. M. (2009). Unraveling sedimentary provenance and tectonothermal history of high to ultrahigh temperature metapelites using zircon and monazite chemistry: A case study from the Eastern Ghats Belt, India. *The Journal of Geology* **117**, 665-683.

van den Kerkhof, A. M. & Hein, U. F. (2001). Fluid inclusion petrography. *Lithos* **55**, 27-47.

van den Kerkhof, A. M., Kronz, A. & Simon, K. (2014). Deciphering fluid inclusions in high-grade rocks. *Geoscience Frontiers* **5**, 683-695.

PUBLICATIONS

1. Chatterjee, A., Das, K., Bose, S., **Ganguly, P**., Hidaka, H., 2017. Zircon U-Pb SHRIMP and monazite EPMA U-Th-total Pb geochronology of granulites of the western boundary, Eastern Ghats Belt, India: new possibility for Neoproterozoic exhumation history, in: Dasgupta, S., Pant, N.C. (Eds.), Crustal evolution of India and Antarctica: the supercontinent connection. *Geological Society London, Special Publication* 457, 105-140.
2. **Ganguly, P**., Bose, S., Das, K., Torimoto, J., Ghosh, G., 2018. Origin of spinel+ quartz assemblage in a Si-undersaturated ultrahigh temperature aluminous granulite and its implication for the PT-fluid history of the Phulbani domain, Eastern Ghats Belt, India. *Journal of Petrology*. https://doi.org/10.1093/petrology/egx078
3. **Ganguly, P**., Das, K., Bose, S., Ghosh, G., Hayasaka, Y., Hidaka, H. U-Pb zircon and U-Th-total Pb monazite ages from the Phulbani Domain of the Eastern Ghats Belt, India: Constraints on high-grade metamorphism and magmatism in the lower crust, *Precambrian Research* (under review).

CONFERENCE PAPERS

1. **Ganguly, P**., Bose, S., Das, K., Ghosh, G., 2016. Field, Microstructural and Electron Backscattered Diffraction (EBSD) study of shear zone rocks from Phulbani, Odisha, Eastern Ghats Belt, India. Presented in the *Annual General Meeting of the Geological Society of India*, IIT Kharagpur,
2. Ghosh, S., Ghosh, G., **Ganguly, P**., Bose, S., Das, K., 2016. Geological significance of the presence of multiple generations of pseudotachylites in Ranipathar Shear Zone, Phulbani domain, Eastern Ghats Belt. Presented in the *Annual General Meeting of the Geological Society of India*, IIT Kharagpur

Table 1. Mineral assemblages, key textural features, mineral compositions, reactions and thermobarometric results of aluminous granulite, migmatitic felsic gneiss, fine-grained charnockite gneiss, coarse-grained charnockite and calc-silicate granulite

Rock types	Mineral assemblages	Key textural features	Reactions	Thermobarometric result	
				Temperature (ºC)	Pressure (kbar)
Aluminous granulite Association A	Grt+Crn+Spl+ Sil+Ilm+Qtz± Kfs±Pl±Bt	Inclusions of Bt_1, Sil_1, Kfs and/or Qtz within Grt_1 and Spl_1; inclusion of Bt_1 and Sil_1 within Crn_1; intergrowth of Spl_2 and Sil_2 at contacts between Grt_1 and Crn_1; intergrowth of Spl_2 and Qtz at the contacts between Grt_1 and Sil_2 (**peak-M_2**); corona of Sil_3 and Grt_2 around Spl_1/Spl_2 (**M_{2R}**) ; corona of Grt_2 around Sil_2 having contacts with Spl_1/Spl_2 (**M_{2R}**); granular and vermicular Crn_2 within Grt_2 and Spl_1/Spl_2. Spl_1: X_{Fe} = 0.66−0.83 Spl_2: X_{Fe} = 0.70−0.72 Grt_1: X_{Fe} = 0.74−0.84 Grt_2: X_{Fe} = 0.76−0.80 Bt_2: X_{Fe} = 0.33−0.37	$Bt_1 + Sil_1$ (± Qtz) → Grt_1 + Kfs + melt Bt_1+Sil_1 (± Ilm_1) → Grt_1+ Crn_1+Spl_1 (Ti- rich Spl_{SS}) ± Kfs + melt Crn_1+ Grt_1 → Spl_2 + Sil_2 $Grt_1 + Sil_1 \rightarrow Spl_3 + Qtz$ $Grt_1 + Sil_2 \rightarrow Spl_2 + Qtz$ $Spl_1/Spl_2 + Qtz \rightarrow Grt_2 + Sil_3$ $Spl_1/Spl_2 + Sil_2 \rightarrow Crn_2 + Grt_2$	Association A: 938-964 (Spl-Sil-Grt-Qtz assemblage) 643-679 (Grt-Bt) 768-790 (Ti-in Bt)	8-8.2
Aluminous Granulite Association B	Grt+Crn+Spl+ Sil+Ilm+Qtz			Association B: 917-945ºC (Spl-Sil-Grt-Qtz assemblage)	7.8-8.1
Migmatitic Felsic gneiss	Grt +Kfs+Bt+Qtz+Pl±Sil	Inclusions of Bt, Kfs and Qtz within porphyroblastic Grt; biotite and sillimanite aggregate at the matrix after porphyroblastic Grt. Grt: X_{Fe} = 0.78−0.81; Bt: X_{Fe} = 0.42−0.55	Grt + Kfs (+Pl) + H_2O → Bt + Sil + Qtz	468-680 (Grt-Bt) 472-713 (Ti-in Bt)	7.4-8.6
Fine-grained charnockite geiss	Opx+Ilm+Kfs+Pl+Qtz +Hbl+Bt+Grt	Corona of Grt and Qtz around Opx/Ilm at contacts with Pl (**M_{2R}**). Grt: $Alm_{72-74}Py_{3-4}Grs_{18-19}$; Bt: X_{Mg} = 0.43-0.47; Hbl: X_{Mg} = 0.34-0.37	Opx ± Ilm + Pl → Grt + Qtz	735-770 (Grt-Opx-Pl-Qtz assemblage)	6.4-6.8
Coarse-grained charnockite	Opx+Ilm+Kfs+Pl +Qtz+Hbl+Bt+Grt	Intergrowth of Grt and Qtz around Opx/Ilm at contacts with Pl (**M_{2R}**). Grt: $Alm_{65-69}Py_{6-8}Grs_{21-24}Sp_{<3}$ Opx: X_{Mg} = 0.27-0.32 Bt: X_{Mg} = 0.60-0.62 Hbl: X_{Mg} = 0.43-0.50	Opx ± Ilm + Pl → Grt + Qtz	681-693 (Grt-Opx-Pl-Qtz assemblage)	6.2
Calc-silicate granulite	Scp+Cpx+Wo+ Pl+Cal+Grt+Qtz	Corona of Grt separating Scp, Cpx, Cal, Pl and Wo (**M_{2R}**) Cpx: X_{Mg} = 0.50-0.63 Scp: X_{Mei} = 0.80−0.83 Grt: andradite (13−29 mole%) and grossular (69−84 mole%) Pl: anorthite (96−99 mole%)	Cpx + Wo ± Scp ± Cal ± O_2 → Grt ± Qtz ± CO_2 Cpx + Wo ± Pl ± Cal ± O_2 → Grt ± Qtz ± CO_2	>800 (Temperature based on X_{Mei})	

Table 2. Mineral assemblages, tectonothermal events and obtained ages from the studied samples of Phulbani domain, EGB.

Rock type	Mineral assemblage	Metamorphic event	Magmatic event	$^{207}Pb/^{206}Pb$ SHRIMP age	EPMA U–Th–total Pb age
Aluminous granulite	Grt+Crn+Spl+ Sil+Ilm+Qtz± Kfs±Pl±Bt	**M_2 (UHT) M_{2R}**		1026±10 to 900±9 Ma from cores of circular to elliptical zircon. Ca.1000 to 1026 Ma- UHT metamorphism (?).	997±13 to 984±7 Ma- time span of UHT metamorphism. 781±15 Ma- development of N-S trending ductile shear zone.
Coarse-grained charnockite	Opx+Ilm+Kfs+Pl+ Qtz+Hbl+Bt+Grt	**M_{2R}**	Charnockite emplacement occurred after M_2 (UHT) metamorphism.	967±5 Ma and 971±18 Ma ^{207}Pb-^{206}Pb mean ages- emplacement ages from oscillatory zoned zircon cores	
Fine-grained charnockite gneiss	Opx+Ilm+Kfs+Pl+ Qtz+Hbl+Bt+Grt	**M_2 (UHT) M_{2R}**		1012±8 to 1024±6 Ma from cores and overgrowths − age of UHT metamorphism (?)	
Migmatitic felsic gneiss	Grt+Kfs+Bt+Qtz+ Pl±Sil				968±4 Ma- from Th- rich oscillatory zoned monazite core- crystallization of melt following UHT.
Felsic augen gneiss	Grt+Kfs +Qtz+Pl±Bt	**M_2 (?)**	Crystallized as granitic magma much prior to the UHT metamorphism and acted as basement for subsequent sediment deposition.	1169±8 Ma ^{207}Pb-^{206}Pb mean ages from the oscillatory zoned zircon cores- emplacement age (age of basement formation?).	1038±13 and 977±11 Ma (^{207}Pb-^{206}Pb spot dates)- UHT metamorphism (?)

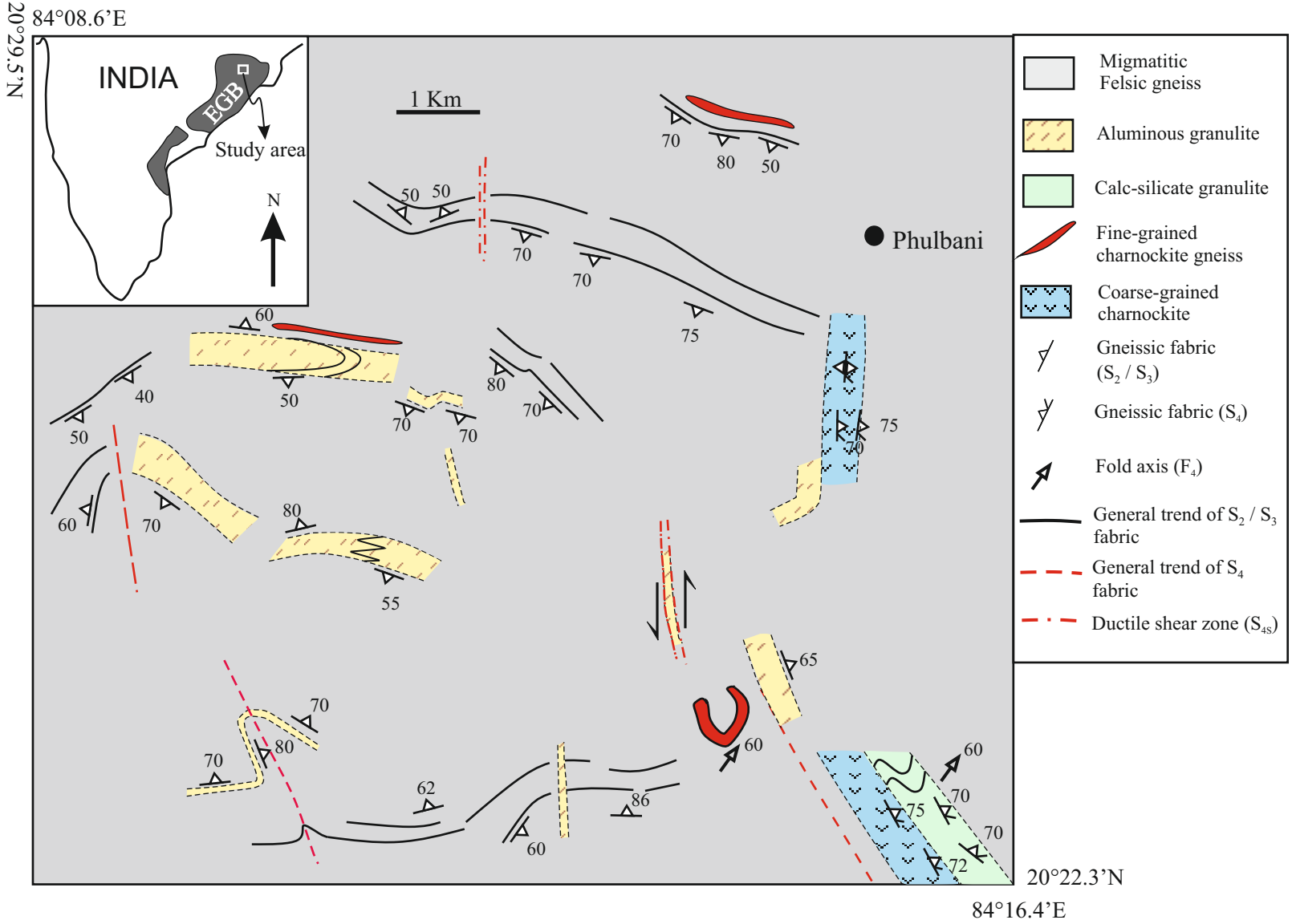

Figure 1. Lithological map of the study area showing major lithological units and their structural elements.

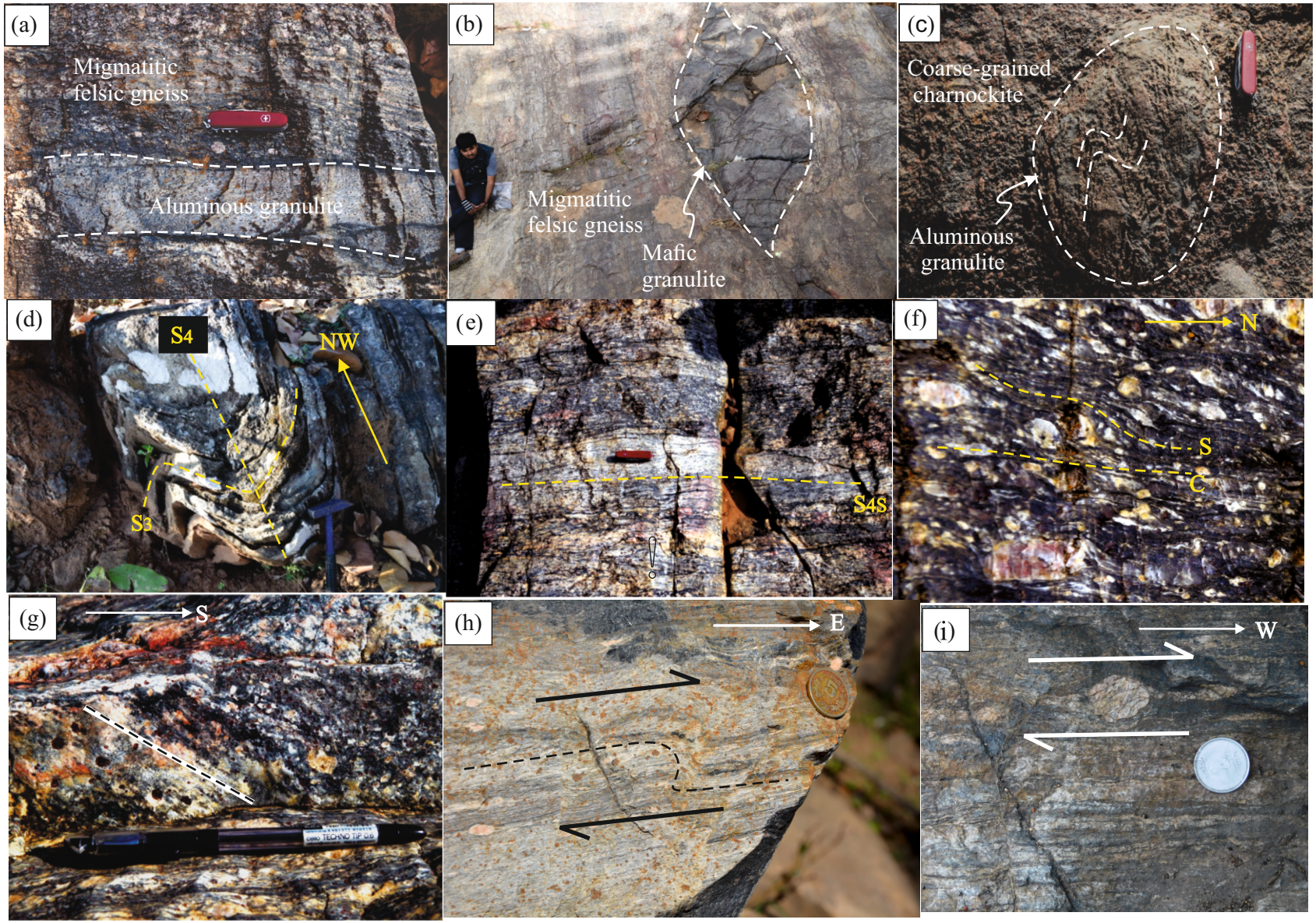

Figure 2. Field photographs of the different lithological units showing outcrop-scale structural features.

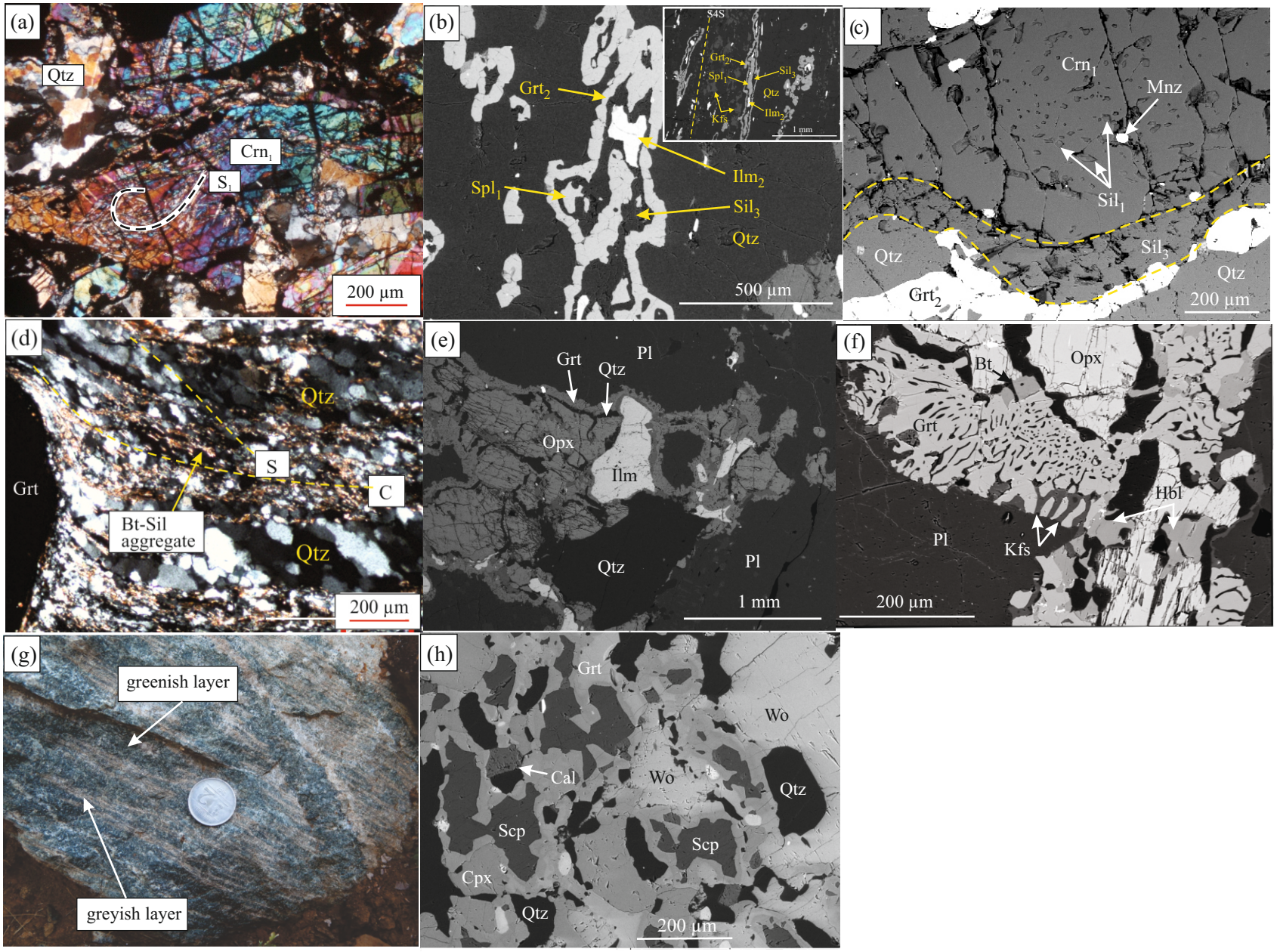

Figure 3. Microphotographs, BSE images and field photograph displaying textural characters of various lithological units in meso- to microscopic scale.

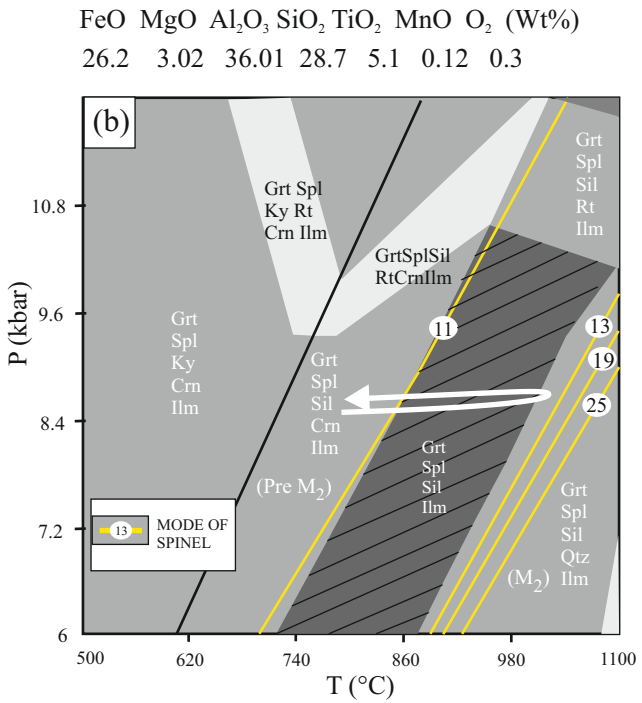

Figure 4. Phase diagram of aluminous granulite showing the transformation from corundum bearing to quartz bearing assemblage.

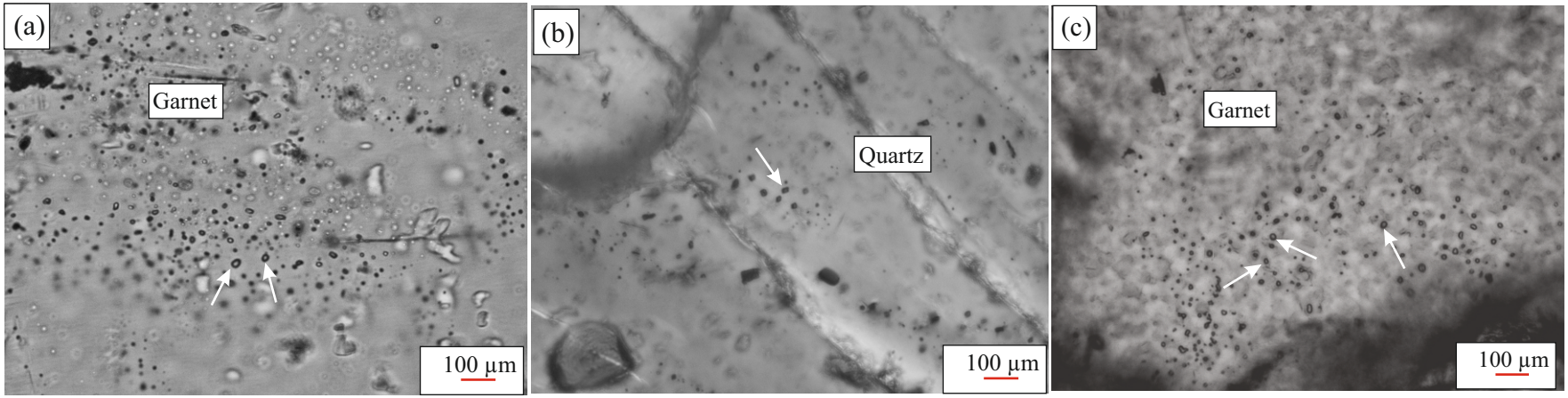

Figure 5. Microphotographs of fluid inclusions present within garnet and quartz in migmatitic felsic gneiss (a, b) and coarse-grained charnockite (c).

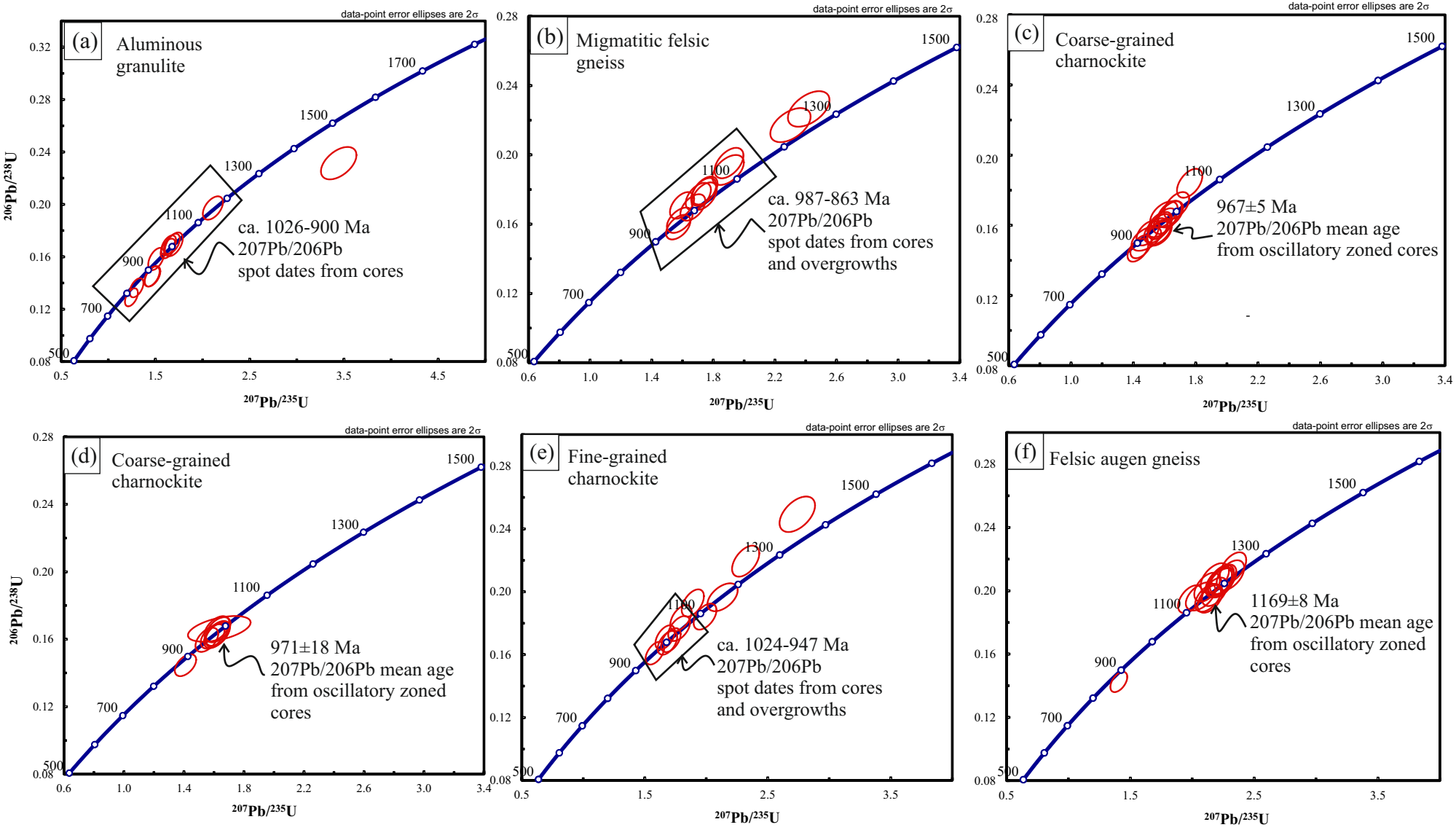

Figure 6. Wetherill plots of the analyzed zircons of the studied samples showing distributions of spot dates and mean ages.

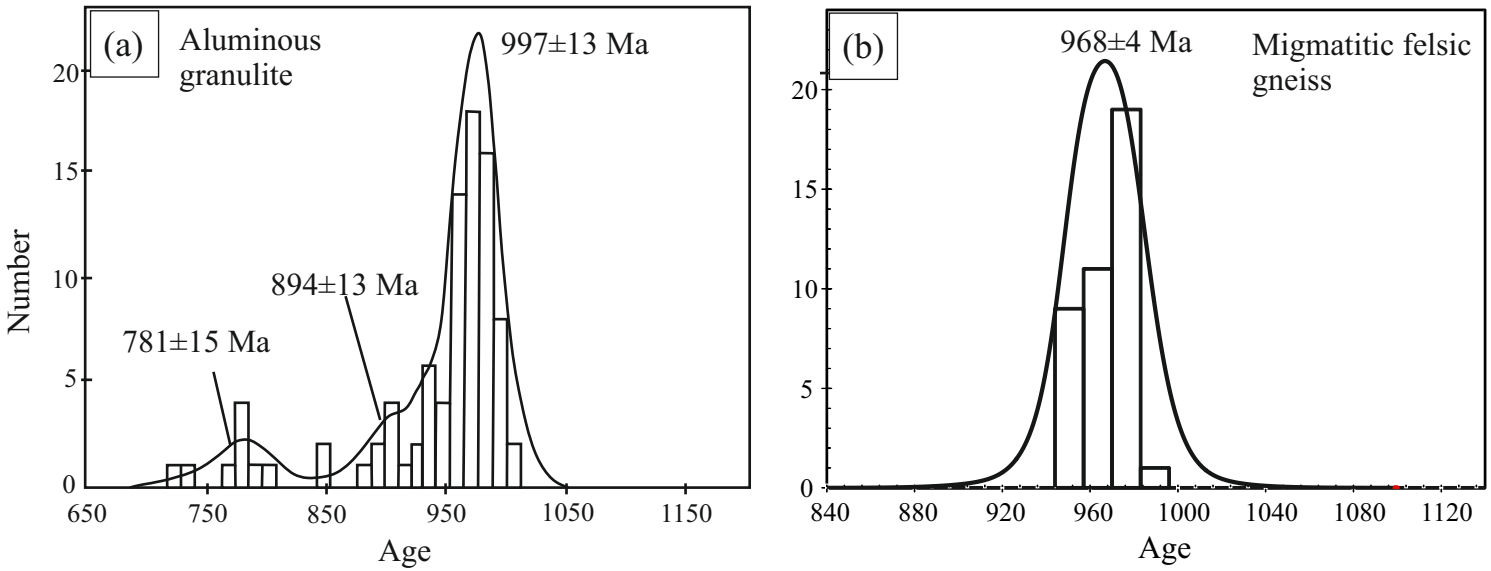

Figure 7. Relative probability density diagrams of the data obtained from the monazite grains.

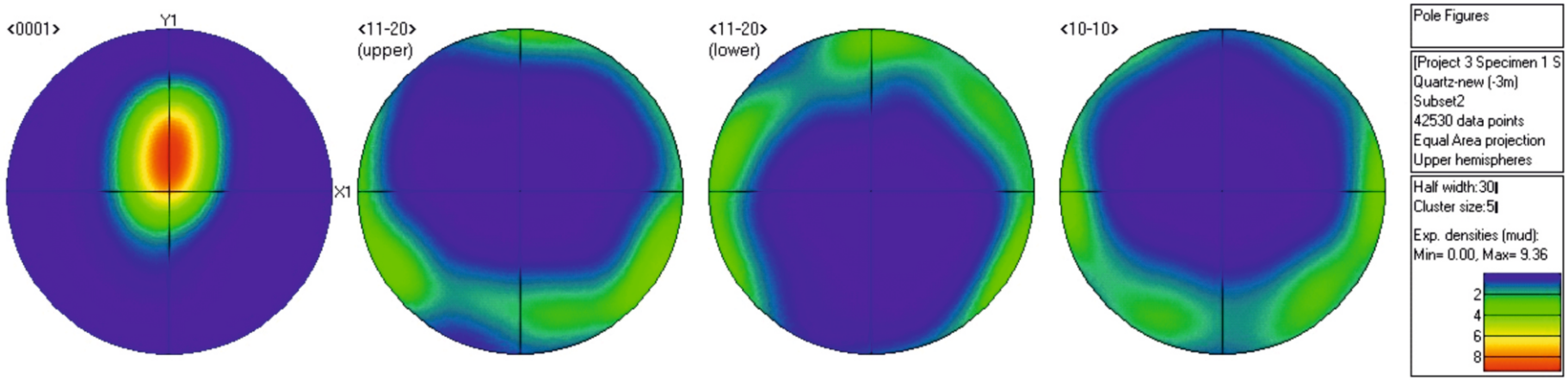

Figure 8. CPO patterns of the deformed quartz grains of migmatitic felsic gneiss obtained by EBSD analysis.

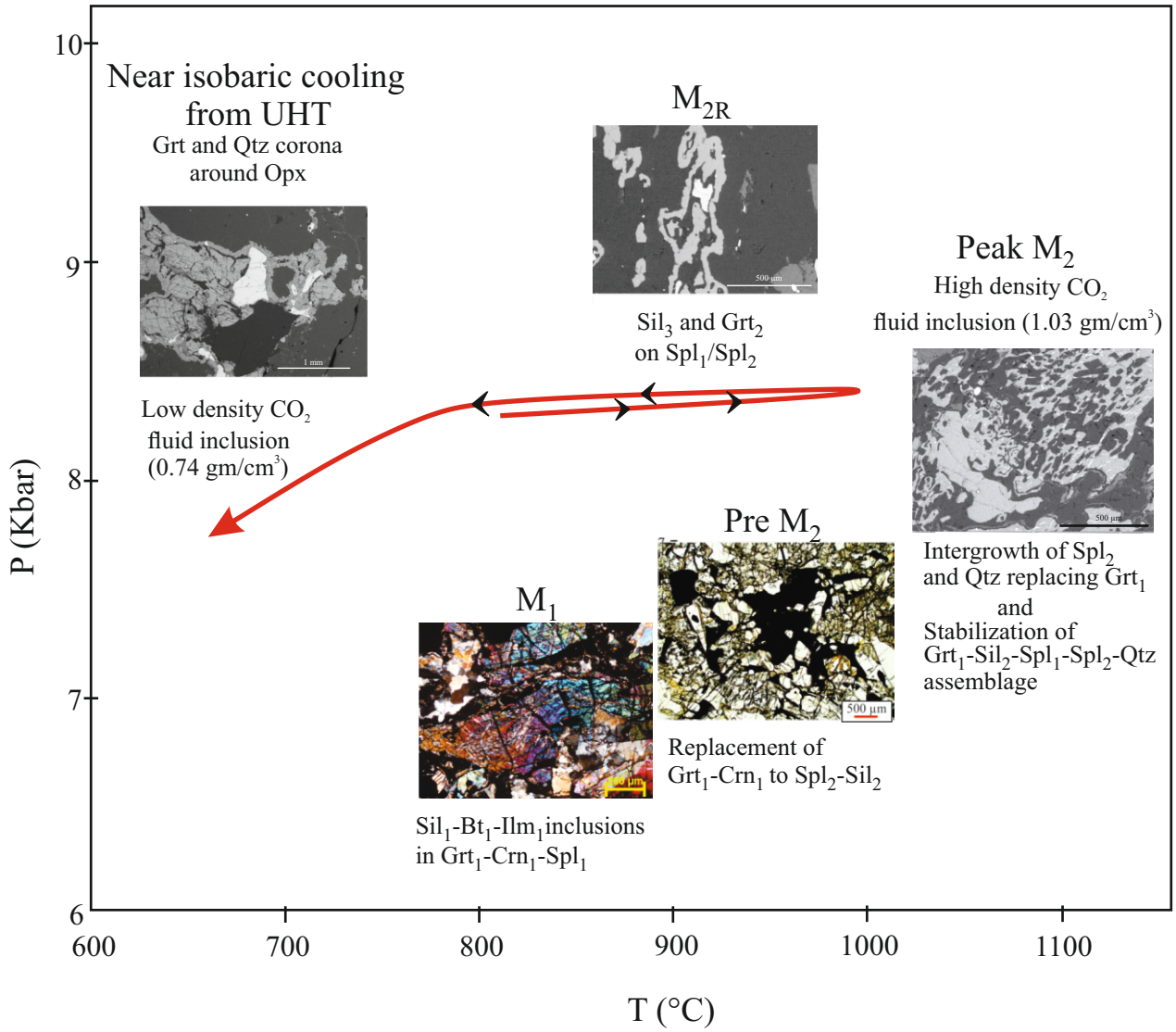

Figure 9. Schematic *P-T* history of the aluminous granulite and associated rocks showing near-isobaric prograde and retrograde path obtained from the textural character, phase diagram modelling, thermobarometry and fluid inclusion data.